Journal of Computational Physics **176,** 330–344 (2002)
doi:10.1006/jcph.2002.6990, available online at http://www.idealibrary.com on IDEAL®

Consistent Boundary Conditions for Multicomponent Real Gas Mixtures Based on Characteristic Waves

Nora Okong'o and Josette Bellan

Jet Propulsion Laboratory, California Institute of Technology, 4800 Oak Grove Drive, MS125-109, Pasadena, California 91109-8099
E-mail: josette.bellan@jpl.nasa.gov

Received September 4, 2001

Previously developed characteristic-wave-based boundary conditions for multicomponent perfect gas mixtures are here extended to real gas mixtures. The characteristic boundary conditions are derived from the one-dimensional wave decomposition of the Euler equations, and the wave amplitude variations are determined from the prescribed boundary conditions on the flow variables. The viscous conditions are applied separately. For multidimensional simulations, the boundary conditions for each coordinate direction are applied additively. These boundary conditions are tested on a representative two-dimensional problem—the propagation of an incompressible vortex by a supersonic flow with outflow conditions specified as nonreflecting—solved using a high-order finite-difference scheme. Simulations conducted for a heptane–nitrogen mixture flow with strong real gas effects display excellent, nonreflective wave behavior as the vortex leaves the computational domain, verifying the suitability of this method for the multidimensional multicomponent real gas flows computed.

Key Words: partial differential equations; fluid mechanics; classical thermodynamics; heat transfer.

CONTENTS

1. INTRODUCTION

Boundary conditions for fluid dynamic equations play a crucial role in determining the character of the solution. Since most fluid dynamic problems of practical interest are

0021-9991/02 $35.00

complex, a solution to the set of differential equations and boundary conditions is usually found numerically rather than analytically. For these types of solutions, Poinsot and Lele [1] distinguish between physical and numerical boundary conditions. The physical boundary conditions are those intrinsically imposed by the problem to be solved. However, for some types of physical problems described by the Euler or Navier–Stokes equations, the number of necessary and sufficient boundary conditions is smaller than the number of primitive variables [1, 2]. In such cases, although the physical boundary conditions are such that the physical problem is well-posed, the numerical problem may be ill-posed, due to the finiteness of the computational domain or due to its discretization, unless numerical boundary conditions can be specified in addition to the physical boundary conditions. Thus, the numerical boundary conditions can be considered as compatibility relations that must be added to the physical boundary conditions to palliate the uncertainty in the variables that are not specified by the physical boundary conditions. These numerical boundary conditions must prevent the introduction of spurious numerical effects, such as wave reflections from a nonreflecting boundary. Of the many boundary schemes that are documented in the literature, we focus on those which have been successfully applied to compressible Navier–Stokes simulations using high-order finite-difference methods. These are generally based on characteristic wave analysis at each boundary point [1, 3–7], with the Reynolds number for viscous flows being considered high enough such that viscous terms can be considered as "corrections" to the mainly hyperbolic nature of the Navier–Stokes equations [2, 8]. These studies were all performed for fluids obeying the perfect gas law, for which thermodynamic variables (notably pressure) are easily computed from the density and internal energy (or temperature).

However, there are many practical applications in which the fluid is not a perfect gas. Such situations occur in high-pressure reactive flows typical of rocket, diesel, or gas turbine engines, as well as in fluid flowing in pipes laid on the ocean floor. These applications provide the motivation to extend perfect gas boundary schemes to real gases. The main difficulty is that for a real gas equation of state (EOS), the complexity of the EOS demands special care in computing thermodynamic variables at the boundaries, constituting an additional computational overhead compared to a perfect gas EOS, as illustrated by Shyue [9]. Furthermore, for the intended application of direct numerical simulation of turbulent flows, we desire a boundary scheme that can easily be coupled to the high-order finite-difference scheme used to discretize the conservation equations, without compromising numerical stability. Based on these considerations, the characteristic-based boundary scheme of Poinsot and Lele [1] is a prime candidate for application to real gas flows, especially since Baum *et al*. [7] have already shown that this method can be extended to multicomponent perfect gas flows. The essence of the method is a local one-dimensional inviscid (LODI) set of equations, described at the boundary in characteristic form. The wave amplitude variation in the characteristic wave formulation is then consistently computed to satisfy the desired boundary conditions. The LODI equations are considered to embody most of the behavior at the boundary, so that the viscous conditions can be applied separately [8].

The present work is devoted to the derivation of accurate and consistent boundary conditions for multicomponent flows where the fluid is a real gas. Section 2 contains the conservation equations for real gas flows, and then the derivation of the boundary conditions. In Section 3, we discuss the generic implementation of these boundary conditions for typical problems encountered in fluid dynamics, and in Section 4, we test the derived boundary

conditions for a heptane–nitrogen mixture with a real gas EOS. Finally, we summarize this work and offer further comments in Section 5.

2. GENERAL EQUATIONS

The conservation equations are the typical compressible Navier–Stokes equations augmented by the species and energy equations

$$\frac{\partial \rho}{\partial t} + \frac{\partial (\rho u_j)}{\partial x_j} = 0, \tag{1}$$

$$\frac{\partial (\rho u_i)}{\partial t} + \frac{\partial (\rho u_i u_j + p\delta_{ij})}{\partial x_j} = \frac{\partial \tau_{ij}}{\partial x_j}, \tag{2}$$

$$\frac{\partial (\rho E_T)}{\partial t} + \frac{\partial [(\rho E_T + p)u_j]}{\partial x_j} = -\frac{\partial q_{IKj}}{\partial x_j} + \frac{\partial (\tau_{ij} u_i)}{\partial x_j}, \tag{3}$$

$$\frac{\partial (\rho Y_\alpha)}{\partial t} + \frac{\partial (\rho Y_\alpha u_j)}{\partial x_j} = -\frac{\partial J_{\alpha j}}{\partial x_j} \quad \text{for } \alpha = 1, N, \tag{4}$$

where t is the time, x_j is the jth coordinate, ρ is the mass density, u_j is the jth velocity component, Y_α is the mass fraction of species α (for N species $\sum_{\beta=1}^{N} Y_\beta = 1$), p is the pressure, and $E_T = E + 1/2 u_i u_i$ is the total energy (internal energy, E, plus kinetic energy). Additionally, τ_{ij} is the Newtonian viscous stress tensor

$$\tau_{ij} = \mu \left[\frac{\partial u_i}{\partial x_j} + \frac{\partial u_j}{\partial x_i} - \frac{2}{3} \frac{\partial u_k}{\partial x_k} \delta_{ij} \right], \tag{5}$$

where μ is the mixture viscosity which is generally a function of the thermodynamic state. The Einstein summation convention (summation over repeated indices) is used for i and j, but not over Greek indices α and β. J_α is the molar flux of species α, and q_{IK} is the Irwing–Kirkwood form of the heat flux [10]. In the species and energy equations, the respective Fick mass diffusion and Fourier heat diffusion terms are now respectively complemented by the Soret and Dufour terms representing the thermal diffusion contribution; therefore J_α and q_{IK} in general contain mass fraction, temperature (T), and pressure gradient terms, as shown by Harstad and Bellan [11–13]. The system of Eqs. (1)–(4) is closed by a real gas EOS, with $N + 2$ thermodynamic variables completely specifying a thermodynamic state.

2.1. Real Gas Thermodynamic Relations

For concreteness, we set the form of the EOS to be $p = p(v, T, Y_1, \ldots, Y_N)$, where v is the molar volume, which is related to the density by $v = m/\rho$. The mixture molar weight is given by $m = \sum m_\alpha X_\alpha$, where m_α and $X_\alpha = mY_\alpha/m_\alpha$ are the molar weight and mole fraction, respectively, of species α. The thermodynamic relations discussed below can all be computed using the EOS.

The isentropic speed of sound is

$$a_s^2 = \frac{1}{\rho \kappa_s}, \tag{6}$$

where κ_s is the isentropic compressibility, which is related to the isothermal compressibility κ_T

$$\kappa_T = -\frac{1}{v(\partial p/\partial v)_{T,Y_\alpha}} \tag{7}$$

by

$$\kappa_s = \kappa_T - vT\alpha_v^2/C_p, \tag{8}$$

where

$$\alpha_v = \frac{1}{v}\left(\frac{\partial v}{\partial T}\right)_{p,Y_\alpha} = -\frac{(\partial p/\partial T)_{v,Y_\alpha}}{v(\partial p/\partial v)_{T,Y_\alpha}} \tag{9}$$

and C_p is the molar heat capacity at constant pressure

$$C_p = \left(\frac{\partial h}{\partial T}\right)_{p,Y_\alpha} = m\left(\frac{\partial H}{\partial T}\right)_{p,Y_\alpha}, \tag{10}$$

with H being the enthalpy per unit mass and h being the enthalpy per mole, $h = mH$

$$H = E + \frac{p}{\rho} = E + \frac{pv}{m}. \tag{11}$$

(The subscript Y_α on a derivative denotes that all the mass fractions are held constant.) The molar heat capacity at constant volume is

$$C_v = m\left(\frac{\partial E}{\partial T}\right)_{v,Y_\alpha} = C_p - \frac{T\alpha_v^2 v}{\kappa_T}. \tag{12}$$

In terms of the partial molar quantities, the enthalpy and molar volume are written as

$$H = \sum_{\alpha=1}^{N} h_\alpha X_\alpha/m = \sum_{\alpha=1}^{N}(h_\alpha/m_\alpha)Y_\alpha; \quad v = \sum_{\alpha=1}^{N} X_\alpha v_\alpha = \sum_{\alpha=1}^{N}(mv_\alpha/m_\alpha)Y_\alpha, \tag{13}$$

where the quantities

$$v_\alpha = (\partial v/\partial X_\alpha)_{T,p,X_\beta(\beta\neq\alpha)} \quad \text{and} \quad h_\alpha = (\partial h/\partial X_\alpha)_{T,p,X_\beta(\beta\neq\alpha)} \tag{14}$$

are the partial molar volume and the partial molar enthalpy.

To derive the boundary conditions, the following internal energy derivatives are required:

$$\left(\frac{\partial E}{\partial \rho}\right)_{p,Y_\alpha} = \frac{1}{\rho}\left[\frac{p}{\rho} - \frac{C_p}{m\alpha_v}\right], \tag{15}$$

$$\left(\frac{\partial E}{\partial p}\right)_{\rho,Y_\alpha} = \frac{C_p\kappa_s}{m\alpha_v} = \frac{C_p}{m\alpha_v}\frac{1}{\rho c^2}, \tag{16}$$

$$\left(\frac{\partial E}{\partial Y_\alpha}\right)_{\substack{\rho,p,Y_\beta \\ \beta\neq\alpha}} = \frac{h_\alpha}{m_\alpha} - \frac{\rho C_p}{m\alpha_v}\frac{v_\alpha}{m_\alpha}. \tag{17}$$

2.2. Perfect Gas Thermodynamic Relations

The perfect gas EOS is

$$p = \rho RT = \frac{R_u T}{v}, \tag{18}$$

and the various thermodynamic quantities are

$$h_\alpha = C_{p,\alpha} T, \quad v_\alpha = v, \tag{19}$$

$$\alpha_v = \frac{1}{T}, \quad \kappa_T = \frac{1}{p}, \quad \kappa_s = \frac{1}{\gamma p}, \tag{20}$$

where $\gamma = C_p / C_v$

$$C_v = C_p - R_u, \quad a_s^2 = \frac{\gamma p}{\rho}. \tag{21}$$

Additionally, the internal energy is

$$E = \frac{C_v}{m} T = \frac{p}{\rho} \frac{1}{(\gamma - 1)}. \tag{22}$$

2.3. Euler Equations Wave Amplitude Variations

To derive the characteristic boundary conditions, we analyze the Euler equations as in Poinsot and Lele [1] and Baum *et al*. [7]. The conservative form of the Euler equations augmented by the species equations is obtained by setting the right-hand sides of Eqs. (1)–(4) to zero. To perform the wave decomposition, we use the Euler equations in primitive form, and the set of primitive variables $\{\rho, u_1, u_2, u_3, p, Y_1, \ldots Y_N\}$. (Note that Poinsot and Lele [1] use p, whereas Baum *et al*. [7] use T as a variable.) We change variables from E to p using Eqs. (15)–(17) to obtain

$$\frac{\partial \rho}{\partial t} + u_j \frac{\partial \rho}{\partial x_j} + \rho \frac{\partial u_j}{\partial x_j} = 0, \tag{23}$$

$$\frac{\partial u_i}{\partial t} + u_j \frac{\partial u_i}{\partial x_j} + \frac{1}{\rho} \frac{\partial p}{\partial x_i} = 0, \tag{24}$$

$$\frac{\partial \rho}{\partial t} + u_j \frac{\partial p}{\partial x_j} + \rho c^2 \frac{\partial u_j}{\partial x_j} = 0, \tag{25}$$

$$\frac{\partial Y_\alpha}{\partial t} + u_j \frac{\partial Y_\alpha}{\partial x_j} = 0, \tag{26}$$

where the speed of sound, c, is given by

$$c^2 = \left(\frac{\partial p}{\partial \rho} \right)_{E, Y_\alpha} + \frac{p}{\rho^2} \left(\frac{\partial p}{\partial E} \right)_{\rho, Y_\alpha} \tag{27}$$

and turns out to be the isentropic speed of sound (a_s).

This set of equations is the same for the perfect gas case, therefore the eigenvalues or wave speeds (λ_i) are the same, as are the wave amplitudes corresponding to each eigenvalue ($\mathcal{L}_i$). Considering only the x_1-direction:

$$\mathcal{L}_1 = (u_1 - c)\left(\frac{\partial p}{\partial x_1} - \rho c \frac{\partial u_1}{\partial x_1}\right) \quad \text{for } \lambda_1 = u_1 - c, \tag{28}$$

$$\mathcal{L}_2 = u_1\left(\frac{\partial p}{\partial x_1} - c^2 \frac{\partial \rho}{\partial x_1}\right) \quad \text{for } \lambda_2 = u_1, \tag{29}$$

$$\mathcal{L}_3 = u_1\left(\frac{\partial u_2}{\partial x_1}\right) \quad \text{for } \lambda_3 = u_1, \tag{30}$$

$$\mathcal{L}_4 = u_1\left(\frac{\partial u_3}{\partial x_1}\right) \quad \text{for } \lambda_4 = u_1, \tag{31}$$

$$\mathcal{L}_{\alpha+4} = u_1\left(\frac{\partial Y_\alpha}{\partial x_1}\right) \quad \text{for } \lambda_{\alpha+4} = u_1, \alpha = 1, N, \tag{32}$$

$$\mathcal{L}_{N+5} = (u_1 + c)\left(\frac{\partial p}{\partial x_1} + \rho c \frac{\partial u_1}{\partial x_1}\right) \quad \text{for } \lambda_{N+5} = u_1 + c. \tag{33}$$

After casting the spatial derivatives in terms of the $\mathcal{L}_i$, the LODI system for the primitive variables containing time- and x_1-derivative terms is

$$\frac{\partial \rho}{\partial t} + \frac{1}{c^2}\left[\frac{(\mathcal{L}_{N+5} + \mathcal{L}_1)}{2} - \mathcal{L}_2\right] = 0, \tag{34}$$

$$\frac{\partial u_1}{\partial t} + \frac{\mathcal{L}_{N+5} - \mathcal{L}_1}{2\rho c} = 0, \tag{35}$$

$$\frac{\partial u_2}{\partial t} + \mathcal{L}_3 = 0, \tag{36}$$

$$\frac{\partial u_3}{\partial t} + \mathcal{L}_4 = 0, \tag{37}$$

$$\frac{\partial p}{\partial t} + \frac{\mathcal{L}_{N+5} + \mathcal{L}_1}{2} = 0, \tag{38}$$

$$\frac{\partial Y_\alpha}{\partial t} + \mathcal{L}_{\alpha+4} = 0; \quad \alpha = 1, N. \tag{39}$$

Depending on the application, a different set of primitive variables may be more convenient for the LODI system. The change of variables is accomplished using thermodynamic relations and the EOS for switching from p to T, as illustrated in the Appendix.

From the above Eqs. (34)–(39), one can find the rate of change of the conservative variables

$$\frac{\partial \rho}{\partial t} + d_1 = 0, \tag{40}$$

$$\frac{\partial \rho u_1}{\partial t} + u_1 d_1 + \rho d_2 = 0, \tag{41}$$

$$\frac{\partial \rho u_2}{\partial t} + u_2 d_1 + \rho d_3 = 0, \tag{42}$$

$$\frac{\partial \rho u_3}{\partial t} + u_3 d_1 + \rho d_4 = 0, \tag{43}$$

$$\frac{\partial \rho E_T}{\partial t} + \left(E_T + \frac{p}{\rho}\right) d_1 + \rho u_i d_{i+1} + \sum_{\alpha=1}^{N} \rho d_{\alpha+4} \left(\frac{\partial E}{\partial Y_\alpha}\right)_{\substack{\rho, p, Y_\beta \\ \beta \neq \alpha}} + \frac{C_p}{m \alpha_v} d_{N+5} = 0, \tag{44}$$

$$\frac{\partial \rho Y_\alpha}{\partial t} + Y_\alpha d_1 + \rho d_{\alpha+4} = 0; \quad \alpha = 1, N, \tag{45}$$

with

$$d_1 = \frac{1}{c^2}\left[\frac{(\mathcal{L}_{N+5} + \mathcal{L}_1)}{2} - \mathcal{L}_2\right] = \rho \frac{\partial u_1}{\partial x_1} + u_1 \frac{\partial \rho}{\partial x_1}, \tag{46}$$

$$d_2 = \left[\frac{\mathcal{L}_{N+5} - \mathcal{L}_1}{2\rho c}\right] = u_1 \frac{\partial u_1}{\partial x_1} + \frac{1}{\rho}\frac{\partial p}{\partial x_1}, \tag{47}$$

$$d_3 = \mathcal{L}_3 = u_1 \frac{\partial u_2}{\partial x_1}, \tag{48}$$

$$d_4 = \mathcal{L}_4 = u_1 \frac{\partial u_3}{\partial x_1}, \tag{49}$$

$$d_{\alpha+4} = \mathcal{L}_{\alpha+4} = u_1 \frac{\partial Y_\alpha}{\partial x_1}, \tag{50}$$

$$d_{N+5} = \frac{\mathcal{L}_2}{c^2} = \frac{u_1}{c^2}\left[\frac{\partial p}{\partial x_1} - c^2 \frac{\partial \rho}{\partial x_1}\right]. \tag{51}$$

3. APPLICATION OF CHARACTERISTIC BOUNDARY CONDITIONS

In the previous section, wave decomposition was used to rewrite the time and spatial derivatives in terms of wave amplitude variations. We distinguish between the outgoing waves which carry information from the interior of the computational domain and which therefore are based on the solution of the conservation equations and the incoming waves which carry information from the exterior of the domain to the region where the solution is sought. The outgoing wave amplitude variations are calculated from the derivatives at the boundary, which are based on the interior points, whereas the incoming wave amplitude variations are determined from the boundary conditions. In the discussion that follows, it is assumed that waves travelling in the $x_1 > 0$ direction exit the computational domain. The definition of incoming and outgoing waves is reversed if waves entering the domain have $\lambda_i < 0$. With this convention, at a (subsonic) boundary where $0 < u_1 < c$, the outgoing wave amplitudes are computed from the interior points, whereas the incoming wave amplitude ($\mathcal{L}_1$ corresponding to $\lambda_1 = u_1 - c$) is derived from the specified boundary conditions. On the other hand, at a (subsonic) boundary where $-c < u_1 < 0$, the incoming wave amplitude variations are set to zero (meaning that there are no waves) except for those that can be derived from the specified boundary conditions, whereas the outgoing wave amplitude variation ($\mathcal{L}_{N+5}$ corresponding to $\lambda_{N+5} = u_1 + c$) is computed from the interior points.

3.1. Subsonic Slip-Wall Boundary Conditions

At slip walls, the normal velocity is zero, i.e., $u_1 = 0$. Then, from Eq. (35), $\mathcal{L}_1 = \mathcal{L}_{N+5}$ and the remaining wave amplitude variations are determined from the interior points using Eqs. (29)–(33).

3.2. Inflow Boundary Conditions

One possibility of specifying inflow conditions is to fix ρ, u_i, and Y_i at the inflow. In this case, the amplitude of incoming waves is set to zero, and ρE_T is updated according to the outgoing wave amplitude variation ($\mathcal{L}_1$ or $\mathcal{L}_{N+5}$) determined from interior points using Eq. (28) or (33).

3.3. Subsonic Nonreflecting Outflow Boundary Conditions

A nonreflecting condition can be imposed by setting the amplitude of incoming waves to zero, i.e., $\mathcal{L}_1 = 0$. Alternatively, the pressure at "infinity" can be used, e.g., through $\mathcal{L}_1 \propto (p - p_\infty)$ [1, 14]. The remaining wave amplitude variations are determined from the interior points using Eqs. (29)–(33).

3.4. Supersonic Outflow Boundary Conditions

In the supersonic case, all the waves are outgoing, so the wave amplitude variations are determined from the interior points using Eqs. (28)–(33).

4. TESTS: HEPTANE–NITROGEN MIXTURES

To test the implementation of the consistent boundary condition based on the characteristic wave method we perform computations for a supercritical two-component nitrogen–heptane flow using Eqs. (1)–(4). The Peng–Robinson EOS, the calculation of thermodynamic quantities from the EOS, and the form of the molar and heat fluxes are described in Miller *et al*. [15]. The equations are solved using fourth-order explicit Runge–Kutta time integration, along with eighth-order finite-differencing and tenth-order explicit spatial filtering of Kennedy and Carpenter [16]. The filter is applied only at interior points to the conservative flow variables in each coordinate direction separately at the end of each time step; for other flow problems, it may be possible to apply the filter less frequently. The implementation of the characteristic boundary condition requires no additional thermodynamic variables or derivatives at the boundary points compared to the interior points—α_v and a_s are computed for determining the time step based on the inviscid CFL condition; the other thermodynamic variables and the derivatives of the primitive variables are used for the calculation of the viscous stresses, heat fluxes, and molar fluxes. We will discuss briefly some one-dimensional acoustic wave propagation tests, then present results for a two-dimensional vortex convection test.

4.1. One-Dimensional Acoustic Wave Propagation

To test the behavior of the boundary scheme at nonreflecting boundaries, a one-dimensional acoustic wave propagation problem was simulated on a two-dimensional domain. Both the wave and its direction of the propagation are perpendicular to that of the subsonic mean flow, with periodic boundary conditions in the streamwise direction. The initial streamwise velocity and temperature are uniform. The viscous conditions are applied as recommended by Poinsot and Lele [1]: for the subsonic outflow, the gradients

of the heat flux and of the shear stresses normal to the boundary are set to zero. This configuration is similar to the initial stages of a supercritical temporal mixing layer simulation, in which strong pressure gradients are caused by the initial vorticity perturbations within the layer. Three cases having either a uniform mass fraction, or a linearly varying (in the cross-stream direction) mass fraction, or a heptane mass source with a Gaussian profile (in the cross-stream direction) where simulated. The mass source is intended to mimic features of mass sources that would arise from chemical reactions or the mass emission (not necessarily evaporation, since at supercritical conditions there is only a single phase) from chunks of supercritical fluid (usually modeled as droplets) in a spray. Due to this heptane mass source term, the mass fraction is increasing with time. In all cases, the acoustic waves exited the domain with minimal reflection. The use of consistent boundary conditions was found to be particularly important in the third test case, where inaccuracies in the boundary conditions, such as introduced by approximate relations derived from the perfect gas EOS, substantially affected the flow evolution throughout the domain.

4.2. Two-Dimensional Vortex in a Uniform Supersonic Flow

Colonius *et al*. [17] discussed the inaccuracies that may occur when one uses one-directionally derived boundary conditions in a two-dimensional setting, especially pressure reflections at nonreflecting boundaries. To test the capability of our consistent-boundary-condition one-dimensional analysis for usage in higher dimension simulations, we adopted the test of a two-dimensional vortical structure propagation. The focus is here on the behavior of the pressure field during the vortex propagation as well as after the vortex exits the domain, the requirement being that the outflow conditions must be satisfactory for the hydrodynamic field as well as for the pressure field. This means that no pressure wave reflection should be detected, even after the vortex exits the domain.

Following the studies of Colonius *et al*. [17] and Poinsot and Lele [1], an incompressible vortex is imposed upon a uniform supersonic flow of velocity $u_1 = U_0$ and Mach number M_0, with uniform temperature T_∞ and uniform heptane mass fraction, $Y_{h,\infty}$. Similar to Poinsot and Lele [1], the vortex is given by the stream function

$$\psi = C \exp\left[-\frac{1}{2}\left(\frac{x_1^2 + x_2^2}{R_c^2}\right)\right], \tag{52}$$

the velocity perturbations are

$$u_1' = \frac{\partial \psi}{\partial x_2}, \quad u_2' = -\frac{\partial \psi}{\partial x_1}, \tag{53}$$

and the pressure is

$$p = p_\infty(1 + w) \tag{54}$$

$$w = [(u_1')^2 + (u_2')^2]^{1/2}. \tag{55}$$

The initial density is computed from the EOS with $T = T_\infty$ and $Y_h = Y_{h,\infty}$. The characteristic boundary conditions are supersonic inflow at $x_1 = 0$ with fixed ρ, u_1, u_2 and Y_h,

and supersonic nonreflecting outflow conditions on the other boundaries, as described in Sections 3.2 and 3.4. Following Poinsot and Lele [1], the viscous conditions are $\partial\tau_{11}/\partial x_1 = 0$ at the inflow, $\partial\tau_{12}/\partial x_1 = 0$, $\partial q_{IK,1}/\partial x_1 = 0$ and $\partial J_{h1}/\partial x_1 = 0$ at the outflow, and $\partial\tau_{12}/\partial x_2 = 0$, $\partial q_{IK,2}/\partial x_2 = 0$ and $\partial J_{h2}/\partial x_2 = 0$ at the lateral boundaries. Here J_h is the heptane molar flux, for which we have adopted the same type of boundary conditions as for the heat flux. The boundary conditions are applied additively at the corners by considering each coordinate direction separately. This approach can be extended in a straightforward manner to three dimensions.

The test case considered has a freestream Mach number of 1.1, a freestream pressure of 60 atm, and the maximum velocity perturbation $w_{\max}/U_0 = 1.5 \times 10^{-3}$. The maximum initial pressure is 102 atm. The initial heptane mass fraction is $Y_{h,\infty} = 0.9$, and the initial temperature is $T_\infty = 600$ K. The domain size is 0.2 m $\times$ 0.2 m with a grid of 120 points in each direction, and the length scale, $2R_c$, is 0.03 m. For these freestream conditions, the compression factor, $Z = p/(\rho R_u T/m)$, is 0.75, and thus this mixture departs considerably from a perfect gas. Contour plots of the vorticity

$$\omega_3 = \frac{\partial u_2}{\partial x_1} - \frac{\partial u_1}{\partial x_2},$$

dilatation

$$\nabla \cdot \mathbf{u} = \frac{\partial u_1}{\partial x_1} + \frac{\partial u_2}{\partial x_2},$$

ρ (kg/m^3), and p (Pa) are presented in Figs. 1–5 at dimensionless times $t^* = tU_0/(2R_c)$ of 0, 2, 4, 6, and 8. Since the center of the vortex reaches the downstream boundary at $t^* = 3.33$, the illustrated time stations encompass a substantial duration after the vortex exits the domain. In all these plots, solid lines denote contours of positive value and dashed lines represent contours of negative value. As the vortex travels in the domain from left to right, the contour plots show that both the vortex and the acoustic waves propagate out of the domain with no discernible reflection, even at the corners.

To assess the circumstances under which the fluid may be modeled as a perfect gas at the boundaries, a similar simulation with $Y_{h,\infty} = 0.5$, $T_\infty = 800$ K was carried out. For these freestream conditions the compression factor, $Z = p/(\rho R_u T/m)$, is 1.02, and therefore this mixture is very close to a perfect gas. It was expected that boundary conditions based on the (simpler) perfect gas EOS would work nearly as well as those based on the real gas EOS. The results using the real gas EOS boundary conditions were similar to those of the test case presented above, namely no discernible reflection of the vortex as it exits the domain. However, computations based on perfect gas EOS boundary conditions were unsuccessful, mainly due to inaccuracies in capturing the mass fraction waves, even though the maximum mass fraction variation was only 2% of the mean mass fraction. This indicates that real gas simulations must be carried out with the corresponding real gas EOS boundary conditions, even when the fluid is essentially a perfect gas. This also shows the necessity of consistent boundary conditions for real gas simulations.

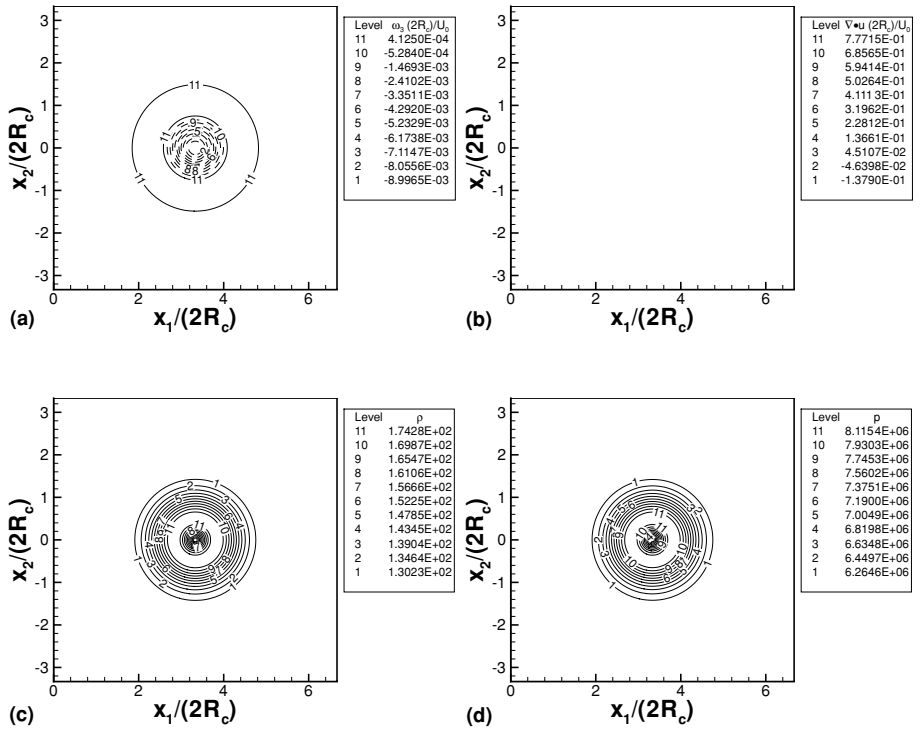

FIG. 1. Propagation of vortex in uniform flow with $Y_{h,\infty} = 0.9$, $T_\infty = 600$ K: Contours of (a) vorticity, (b) dilatation, (c) density (kg/m^3), and (d) pressure (Pa) at $tU_0/(2R_c) = 0$.

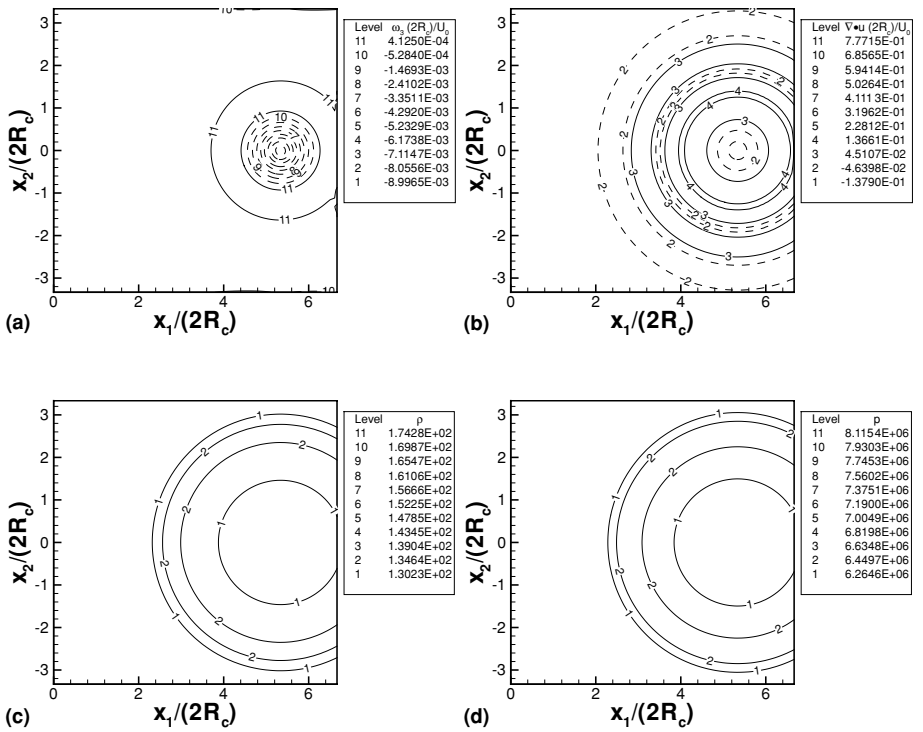

FIG. 2. Propagation of vortex in uniform flow with $Y_{h,\infty} = 0.9$, $T_\infty = 600$ K: Contours of (a) vorticity, (b) dilatation, (c) density (kg/m^3), and (d) pressure (Pa) at $tU_0/(2R_c) = 2$.

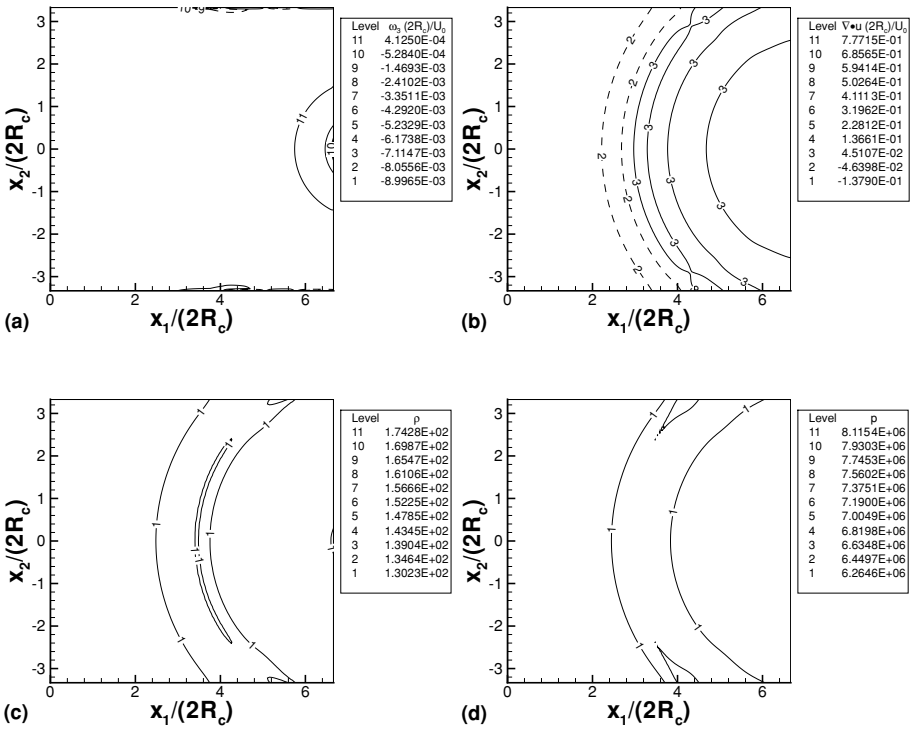

FIG. 3. Propagation of vortex in uniform flow with $Y_{h,\infty} = 0.9$, $T_\infty = 600$ K: Contours of (a) vorticity, (b) dilatation, (c) density (kg/m^3), and (d) pressure (Pa) at $tU_0/(2R_c) = 4$.

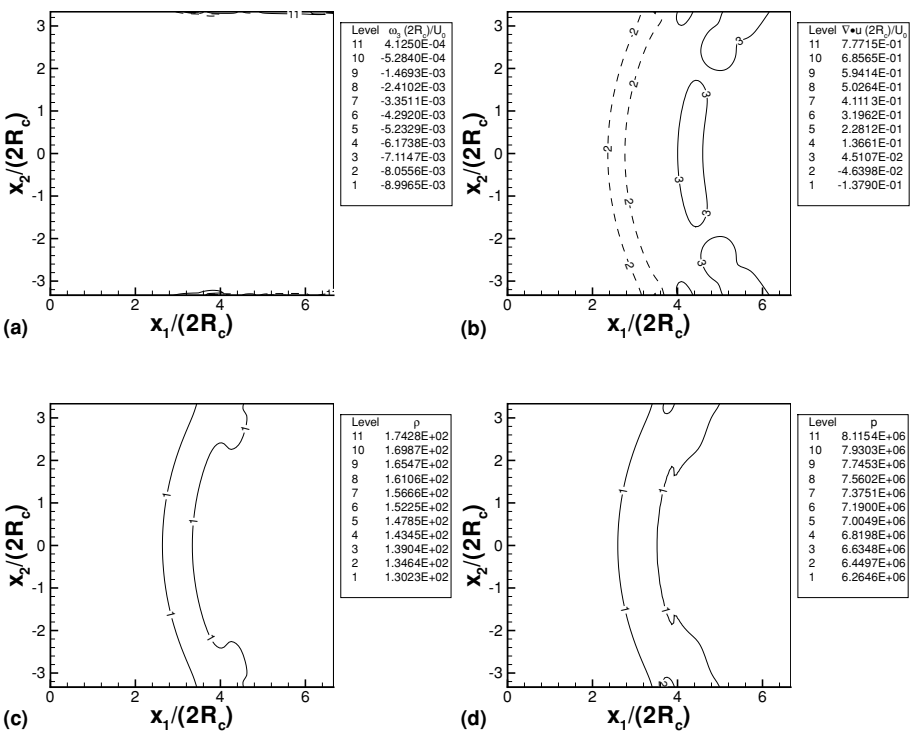

FIG. 4. Propagation of vortex in uniform flow with $Y_{h,\infty} = 0.9$, $T_\infty = 600$ K: Contours of (a) vorticity, (b) dilatation, (c) density (kg/m^3), and (d) pressure (Pa) at $tU_0/(2R_c) = 6$.

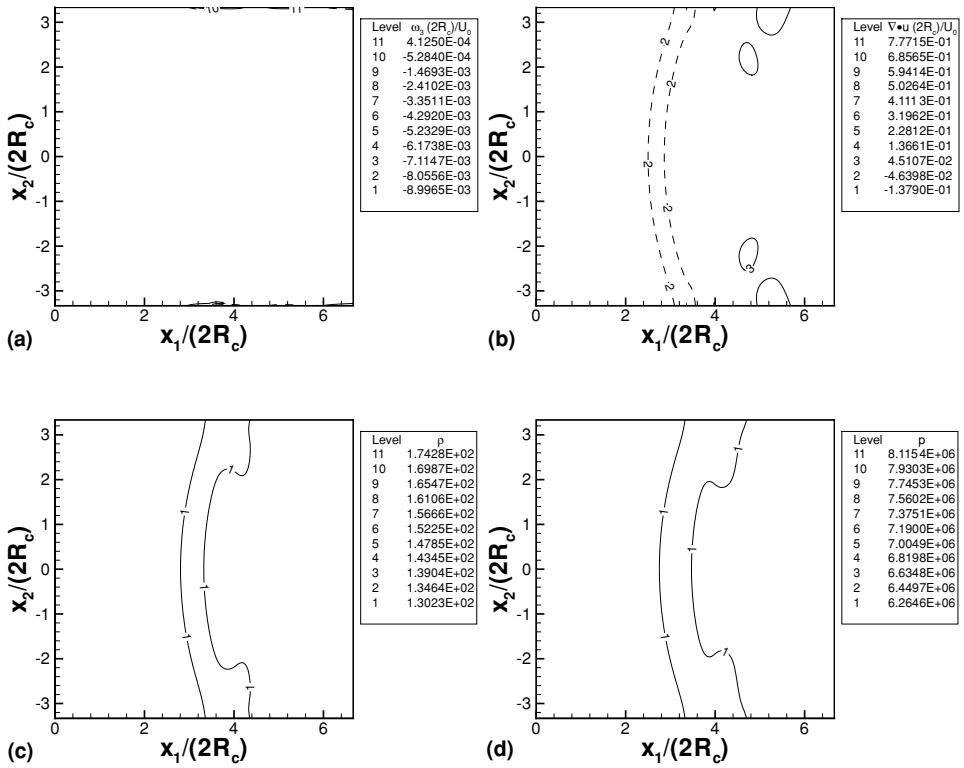

FIG. 5. Propagation of vortex in uniform flow with $Y_{h,\infty} = 0.9$, $T_\infty = 600$ K: Contours of (a) vorticity, (b) dilatation, (c) density (kg/m^3), and (d) pressure (Pa) at $tU_0/(2R_c) = 8$.

5. CONCLUSIONS

Consistent boundary conditions based on characteristic wave analysis were here derived for multicomponent flows governed by real gas equations of state. The characteristic wave analysis was used to develop a local one-dimensional inviscid system, which was used to impose inviscid boundary conditions based on the desired behavior of waves at the boundary. Appropriate wave amplitude variations for inflow and nonreflecting outflow boundary conditions were described. The viscous conditions were imposed separately; chemical source terms can also be considered in a similar manner. For multidimensional flow configurations, the boundary conditions for each variable were additively applied for each direction, making this method suitable for both two- and three-dimensional simulations. This method can therefore be applied to direct numerical simulations of turbulent reacting real gas flows.

The boundary conditions have been successfully applied to both one-dimensional and two-dimensional viscous problems. The two-dimensional problem consisted of the propagation of an incompressible vortex by a supersonic flow. In this simulation, nonreflecting conditions were used at the outflow and lateral boundaries. The fluid was a high-pressure heptane–nitrogen mixture, described by a real gas equation of state. The conservation equations were solved using fourth-order Runge–Kutta explicit time integration and eighth-order explicit finite differencing. Demonstrating the suitability of this boundary condition method for this flow configuration, the vortex and the waves it generated exited the domain without reflection.

APPENDIX: WAVE AMPLITUDES USING TEMPERATURE

The specification of the wave amplitudes, $\mathcal{L}_i$ of Eqs. (28)–(33), in terms of temperature is most conveniently accomplished by using the EOS to express the pressure gradient in terms of the density, temperature, and N mass fractions as

$$\frac{\partial p}{\partial x_1} = \frac{1}{\rho\kappa_T}\frac{\partial \rho}{\partial x_1} + \frac{\alpha_v}{\kappa_T}\frac{\partial T}{\partial x_1} + \frac{1}{\kappa_T}\sum_{\alpha=1}^{N}\frac{\rho v_\alpha}{m_\alpha}\frac{\partial Y_\alpha}{\partial x_1}. \tag{A.1}$$

The local one-dimensional inviscid (LODI) equation for the temperature is

$$\frac{\partial T}{\partial t} + \frac{mT\alpha_v(\mathcal{L}_{N+5} + \mathcal{L}_1)}{2\rho C_p} + \frac{\mathcal{L}_2}{\rho\alpha_v c^2} - \frac{1}{\alpha_v}\sum_{\alpha=1}^{N}\frac{\rho v_\alpha}{m_\alpha}\mathcal{L}_{\alpha+4} = 0. \tag{A.2}$$

ACKNOWLEDGMENTS

This study was conducted at the Jet Propulsion Laboratory (JPL) and sponsored jointly by the Air Force Office of Scientific Research under the direction of Dr. Julian Tishkoff and by the Army Research Office under the direction of Dr. David Mann under an interagency agreement with the National Aeronautics and Space Administration. The authors thank Dr. Kenneth Harstad of JPL for helpful discussions on real gas thermodynamics. The computational resources were provided by the JPL Supercomputing Center.

REFERENCES

1. T. J. Poinsot and S. K. Lele, Boundary conditions for direct simulations of compressible viscous flows, *J. Comput. Phys.* **101**, 104 (1992).
2. P. Dutt, Stable boundary conditions and difference schemes for Navier–Stokes equations, *SIAM J. Numer. Anal.* **25**(2), 245 (1988).
3. H.-O. Kreiss, Initial boundary value problems for hyperbolic systems, *Comm. Pure Appl. Math.* **23**(3), 277 (1970).
4. B. Engquist and A. Majda, Absorbing boundary conditions for numerical simulations of waves, *Math. Comp.* **31**(139), 629 (1977).
5. R. Higdon, Initial-boundary value problems for linear hyperbolic systems, *SIAM Rev.* **28**(2), 177 (1986).
6. K. Thompson, Time dependent boundary conditions for hyperbolic systems, *J. Comput. Phys.* **68**, 1 (1987).
7. M. Baum, T. Poinsot, and D. Thevenin, Accurate boundary conditions for multicomponent reactive flows, *J. Comput. Phys.* **116**, 247 (1994).
8. B. Gustafsson and A. Sundstrom, Incompletely parabolic problems in fluid dynamics, *SIAM J. Appl. Math.* **35**(2), 343 (1978).
9. K.-M. Shyue, A fluid-mixture type algorithm for compressible multicomponent flow with van der Waals equation of state, *J. Comput. Phys.* **156**, 43 (1999).
10. S. Sarman and D. J. Evans, Heat flux and mass diffusion in binary Lennard–Jones mixtures, *Phys. Rev. A*, **45**(4), 2370 (1992).
11. K. Harstad and J. Bellan, Isolated fluid oxygen drop behavior in fluid hydrogen at rocket chamber pressures, *Int. J. Heat Mass Transfer* **41**, 3537 (1998).
12. K. Harstad and J. Bellan, A validated all-pressure fluid drop model for binary mixtures: Heptane in nitrogen, Technical Report AIAA 99-206 (AIAA/ASME/SAE Propulsion Meeting, 1999).
13. K. Harstad and J. Bellan, An all-pressure fluid-drop model applied to a binary mixture: Heptane in nitrogen. *Int. J. Multiphase Flow* **26**(10), 1675 (2000).

14. D. H. Rudy and J. C. Strikwerda, A nonreflecting outflow boundary condition for subsonic Navier–Stokes calculations, *J. Comput. Phys.* **36**, 55 (1980).
15. R. Miller, K. Harstad, and J. Bellan, Direct numerical simulations of supercritical fluid mixing layers applied to heptane-nitrogen, *J. Fluid Mech.* **436**, 1 (2001).
16. C. A. Kennedy and M. H. Carpenter, Several new numerical methods for compressible shear layer simulations, *Appl. Numer. Math.* **14**, 397 (1994).
17. T. Colonius, S. Lele, and P. Moin, Boundary conditions for direct computation of aerodynamic sound generation. *AIAA J.* **31**(9), 1574 (1993).